Desalination and Water Treatment
www.deswater.com

doi: 10.1080/19443994.2015.1091994

57 (2016) 18463–18474
August

Taylor & Francis
Taylor & Francis Group

Chitosan-/PVA-coated magnetic nanoparticles for Cu(II) ions adsorption

Aylin Altinisik, Kadir Yurdakoc*

Science Faculty, Chemistry Department, Dokuz Eylül University, 35390 Buca, Izmir, Turkey, email: aylin.altinisik@deu.edu.tr (A. Altinisik), Tel. +90 23230198695; email: k.yurdakoc@deu.edu.tr (K. Yurdakoc)

Received 28 February 2015; Accepted 26 August 2015

ABSTRACT

The magnetic chitosan/PVA/iron oxide nanoparticles have been synthesized for the usage of Cu(II) ions removal from aqueous solution. The structure and morphology of the adsorbent was investigated by X-Ray diffraction, scanning electron microscope, and Fourier transform infrared analyses. Adsorption performances of the adsorbents were tested as a function of Cu (II) ion concentration, pH value, time, and temperature. The adsorption kinetics and isotherms were analyzed by Lagergren first-order, pseudo-second-order, Elovich equation, intra-particle diffusion models, and Langmuir, Freundlich, DR and BET isotherms, respectively. The kinetics results pointed out pseudo-second-order. Maximum sorption capacity of the adsorbent was estimated to be 500 mg/g at pH 5.0. Thermodynamic parameters such as Gibbs free energy (ΔG°), enthalpy (ΔH°), and entropy (ΔS°) changes were also determined and indicated that the sorption process was endothermic in nature. The magnetic results showed that the adsorbent can be manipulated by an external magnet with sufficient separation. The process is clean, safe, and easy enough for the removal of Cu(II) ions.

Keywords: Magnetic chitosan; Biosorption; Copper; Isotherm; Biosorbent

1. Introduction

Recently, the heavy metal pollution increases with the developing industrial technology. Industrial wastewater contains a considerable amount of heavy metal ions and organic pollutants, which, even in low concentration, can cause several health problems in animals and human beings. Today, several methods have been developed for the removal of heavy metal pollution from wastewater, such as solvent extraction, chemical precipitation, ion exchange, adsorption, electrodialysis, and membrane technologies [1,2]. Adsorption is the most applicable option, both technically and economically among these methods. In the adsorption techniques, many materials have been used as adsorbent; however, biosorbents seem to be an attractive approach due to readily available, economic, and environmentally compatible properties [3].

Among the common biosorbents, chitosan (CS) is still considered as a potential due to its functional groups which can interact with the metal ions by its hydroxyl and amino groups on the chain backbone [4–6]. Now, lots of different CS derivatives have been developed against metal ions such as Cu(II), Cd(II), Pb(II), Hg(II), Ni(II), and Cr(VI) [7–10].

The separation of the adsorbents from the solution using traditional filtration and sedimentation may result in blocking the filters or loss of adsorbent and cause secondary pollution [11]. Magnetic particles, Fe_2O_3, Fe_3O_4, and ferrites have been recently developed providing quick and effective separation of the

*Corresponding author.

adsorbent by an external magnet from the solution [12–19]. These nanoparticles in general showed a high surface area, but their magnetic reply was relatively low. For this reason, nanospheres and core–shell-structured magnetic nanoparticles were constructed for separating the adsorbent from aqueous solution in short-time duration. Magnetic separation technologies by the combination of chitosan and magnetic compounds are an efficient strategy to overcome this problem. The magnetic adsorption techniques as convenient, rapid, low cost, and amenable to automation methods, have received considerable attention [20–22]. Magnetic core–chitosan shell materials were widely synthesized and used for wastewater treatment. Magnetite is used as magnetic cores because of its well-known synthesis methods, strong magnetic property, and also low toxicity [23,24].

On the other hand, Cu(II) ion contamination sources in the environment are coming from the wastes of fertilizer, electrical, metal electroplating, paint, pigment, and wood manufacturing industries [25–28]. Adsorption of Cu(II) onto chitosan bound Fe_3O_4 nanoparticles [29], gum arabic/Fe_3O_4 adsorbent [30], 1,6-hexadiamine-modified Fe_3O_4 [31], goethite and hematite nanoparticles [32], chitosan [33–36], chitosan-coated PVC beads [37], cross-linked chitosan and chitosan acetate crown ethers [36,38], chemically modified chitosan [39], polymer-modified activated carbon [40], carbon nanotubes [41], amino-functionalized magnetic nanoparticles [31], silica gel matrix composite [42], and magnetic chitosan composite bead [43] were studied. The results were shown by Langmuir isotherm with the maximum adsorption capacities over the ranges of 17–196 mg/g at pH 2–6 at 298 K, and 98% removal efficiency was achieved [29–43].

In the present study, a novel magnetic chitosan/PVA/iron oxide nanoparticles (CNP) acting as an adsorbent with high adsorption capacity was designed. The coating of magnetite NPs with CS/PVA improves the chemical stability of nanoparticles, preventing their oxidation and coagulation. The synthesized CNP adsorbents were characterized. Their adsorption properties and their reusability were also investigated for Cu(II) ions.

2. Materials and methods

2.1. Material

Chitosan (viscosity; 400 mPa.s, 1% in acetic acid at 20˚C, 48,165 Sigma) and poly(vinyl alcohol) (Mn = 72,000; 97.5–99.5 mol% hydrolysis, 81,384 Sigma) were purchased from Sigma–Aldrich. $FeCl_3{\cdot}6H_2O$ (Riedel-de Haën, 12,319), $FeSO_4{\cdot}7H_2O$ (Merck, AM0526865 328), and NH_3 (32%, Merck, B916626 638) were used in the preparation of nanoparticles. The chemical agents were all analytical grade. Double-distilled water was used in the experiments.

2.2. Preparation of Fe_3O_4 (NP) nanoparticles

Fe_3O_4 (NP) nanoparticles were prepared by co-precipitation of Fe^{2+} and Fe^{3+} salts. 0.027 mol of $FeCl_3{\cdot}6H_2O$ and 0.0055 mol of $FeSO_4{\cdot}7H_2O$ were dissolved in deoxidized double-distilled water. Chemical precipitation was achieved by adding dropwise 40 mL of NH_3 solution (32%) to this solution in ultrasonic bath at 40˚C for 20 min under the protection of N_2 gas. The temperature of the solution was raised to 60˚C and maintained constant for another 5 h. During the reaction, additional NH_3 solution (6.6 mL) was added to complete the precipitation. After cooling to room temperature, NPs were magnetically separated from the aqueous solution by an external magnet. Then, the final product was washed several times with water and ethanol, and freeze dried.

2.3. Preparation of CNP

The CNP with CS: PVA: NP as 1:1:1 weight ratio was prepared. Chitosan was dissolved in 2% (v/v) aqueous acetic acid. PVA powder was dissolved in double-distilled water under mechanical stirring at 80˚C. Then, PVA solution was mixed with chitosan solution. Then, NP was added to this homogeneous mixture with vigorous stirring in ultrasonic bath for 3.0 h at 30˚C. The resulting solution was dropped through a needle into a sodium hydroxide bath (0.1 M) for the formation of hydrogel beads. The magnetic CS/PVA hydrogel beads were then obtained by washing with water for several times and finally freeze dried.

2.4. Characterization of the samples

The NP and CNP were characterized by Fourier transform infrared (FTIR) spectroscopy. FTIR was used to investigate the interaction of Chitosan, PVA, and NP. FTIR spectra were recorded by a Perkin-Elmer FTIR spectrophotometer Spectrum BX-II in the range 4,000–400 cm^{-1} with the sum of 20 scans at a resolution of 4 cm^{-1}.

X-Ray diffraction (XRD) patterns of the NP and CNP were recorded on a Philips X-Pert Pro X-Ray diffractometer using Cu K_α radiation at 45 kV and

40 mA. The scanning scope of 2θ was ranged from 5 to 50°C.

The thermal properties of the prepared samples were analyzed with a Perkin-Elmer Diamond TG/DTA instrument. TG/DTG profiles were performed from 30 to 600°C at a heating rate of 10°C/min under N_2 flow of 10 mL/min.

The morphology of the samples was monitored by scanning electron microscopy (SEM). The images were obtained using 10 kV accelerating voltage. SEM images were taken at different magnifications (in the range of 1,000× and 10,000×) using FEI Quanta 250 FEG SEM instrument.

The magnetic properties of the samples were measured on a vibrating sample magnetometer (VSM) (Cryogenic Limited PPMS) at room temperature. Specifications of the VSM magnetometer are as follows: magnet type: NbTi Coil; magnetic field range: up to ±5 *T*; sample temperature range: 2–325 K; typical cooling rate: 1 K/min; maximum sample size: 10 mm × 10 mm × 1 mm.

2.5. Adsorption studies

Batch adsorption method was carried out by mixing 0.01 g of CNP with 15 mL Cu(II) ion solutions of different concentrations (100–400 mg/L) at a constant temperature bath (30°C). After equilibrium, the adsorbent was separated from the aqueous phase by a magnet. The concentration of Cu(II) in the supernatant was determined by Perkin-Elmer AAnalyst 700 Model atomic absorption spectrophotometer (AAS) at 249.2 nm.

The amount of Cu(II) adsorbed per g of CNP in the equilibrium, q_e (mg/g) was calculated using Eq. (1):

$$q_e = (C_0 - C_e)/m \times V \quad (1)$$

where C_0 and C_e are the initial and equilibrium Cu(II) ion concentrations in mg/L, respectively. V is the volume of the solution (L) and m (g) is the mass of the CNP. The experiments were performed at 288, 298, 308, and 318 K in a shaking water bath at 150 rpm.

2.6. Kinetic studies

Kinetic measurements were carried out using 0.01 g CNP and 15 mL of Cu(II) solution at a shaking constant temperature bath as in adsorption experiments. The Cu(II) ion concentration was analyzed spectrophotometrically as before at definite interval of time.

2.7. Effect of pH on adsorption

The effect of pH on adsorption was studied at pH values of 2–6 intervals. The pH values of Cu(II) solutions were adjusted by HCl or NaOH solutions. Initial Cu(II) ion concentration, shaking time, temperature, and the amount of adsorbent were chosen as 500 mg/L, 180 min, 298 K, and 0.01 g, respectively.

2.8. Multiple adsorption/desorption cycles (reusability of CNP)

In the reusability experiments, CNP were treated with 10^{-2}–10^{-5} M HNO_3 solutions. The desorption percentage of Cu(II) was calculated from the Eq. (2):

$$\text{Desorption Percentage} = m_d/m_s \times 100 \quad (2)$$

where m_d and m_s are Cu(II) ions desorbed and adsorbed as mg, respectively.

The Cu(II) concentrations were determined by AAS after removing the CNP from the desorption medium. Five consecutive adsorption–desorption cycles were conducted for Cu(II), adsorption of corresponding metal ions from 500 mg/mL for 180 min. Each time, the adsorption and desorption amounts were determined.

3. Results and discussions

3.1. Characterization of CNP

3.1.1. FTIR analysis

FTIR spectra of NP and CNP are shown in Fig. 1. It can be seen clearly, the band at 579 cm^{-1} is attributed to Fe_3O_4 particles. The absorption bands around 1,640 and 1,560 cm^{-1} are referred to asymmetric C=O stretching (amide I) and N–H bending (amide II) of acetamido groups, respectively. The interaction between CS and PVA may illuminate by the change in the characteristic shape of the CS spectra as well as shifting of band to a lower frequency range due to hydrogen bonding between –OH of PVA and –OH or NH_2 of chitosan.

Meanwhile, there would also be shifting at the broad band above 3,400 cm^{-1} corresponding to O–H and N–H bonds. Moreover, compared with FT-IR spectra of pure CS membrane, the absorption band of CNP at 1,255 cm^{-1} disappeared. These results suggested the formation of hydrogen bond between CS and PVA molecules [44–46]. To determine the blending ratio, a baseline was drawn with reference to –CH stretching (by PVA) around 2,945 cm^{-1} and the ratio

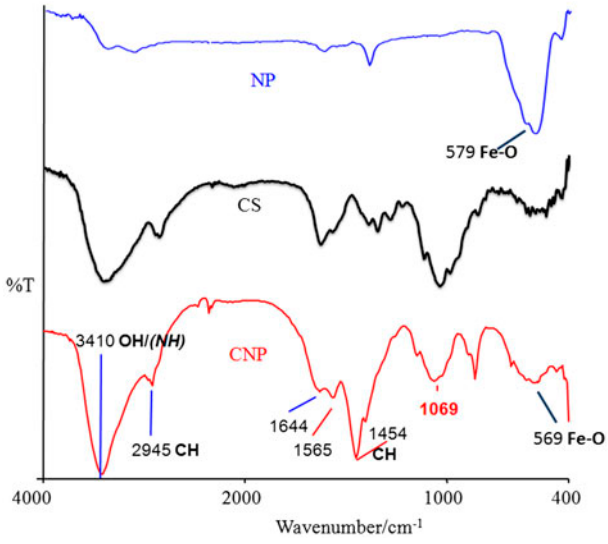

Fig. 1. FTIR spectrum of CS, NP, and CNP.

of absorption was made with respect to 1,565 cm^{-1}. A graph was plotted between chitosan and PVA concentration vs. 1,565/2,945 cm^{-1} ratios (Fig. 1), whose regression coefficient was found to be 0.76 [47].

3.1.2. SEM analysis

SEM images are used to characterize the morphology and size of NP and CNP (Fig. 2). According to the SEM images, it has been observed that NP morphology is continuous, spherical, uniform, and individual particles with a diameter of 10 nm with a magnification value of 400,000×. On the other hand, morphology of the CNP is not uniform as compared with NP. However, the average particle size was measured from the SEM images as approximately 26 nm with a magnification value of 100,000×. Due to the increase in particles size, it can be said that NP has been encapsulated by CS/PVA. Also, it was corroborated by the other characterization analysis at the other parts.

3.1.3. XRD analysis

XRD patterns of NP and CNP are given in Fig. 3. The peaks at 2θ values of 30.32˚, 35.64˚, 43.36˚, 53.66˚, 57.26˚, and 62.87˚ were related with the (2 2 0), (3 1 1), (4 0 0), (4 2 2), (5 1 1), and (4 4 0) crystal planes of Fe_3O_4 [48–50]. In the view of such information, it can be clearly seen that all the characteristic peaks of Fe_3O_4 could be appeared in the patterns of NP and CNP besides the diffraction peak at 22˚ associated with chitosan/PVA blend.

In accordance with Debye–Scherrer equation, the uncoated NP and NP particles in CNP had an average diameter of 7 nm which was appropriate to SEM result for NP. Also, according to the crystallinity (CrI), CrI of the pure chitosan has increased from 45.4 to 74.5% by synthesized CNP form [5,51].

These results demonstrated that the CNP have been synthesized successfully by conserving the crystal structure of NP.

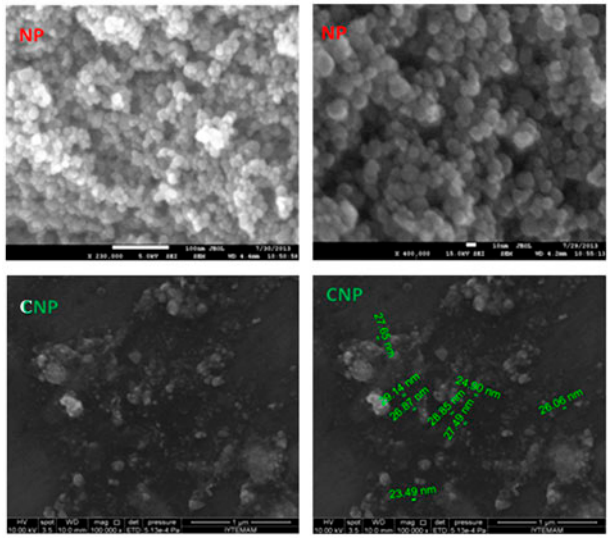

Fig. 2. SEM images of NP and CNP.

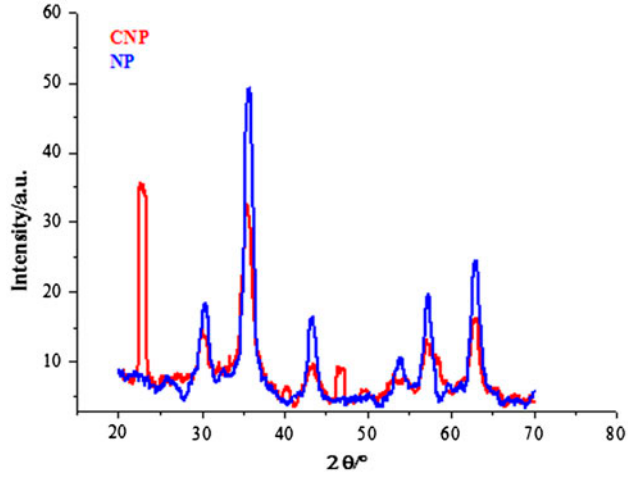

Fig. 3. XRD patterns of the NP and CNP.

3.1.4. TG/DTG analysis

The decomposition temperatures were determined by TG analysis as shown in Fig. 4(a) and (b) for NP and CNP, respectively. There is only one step of 3% mass loss which pertains to moisture for NP. On the other hand, considering the thermograms of CNP, one-step main mass loss was observed at 308°C in Fig. 4(b). This degradation (24%) refers to the degradation of coated polymer. It is obvious that thermal stability of NP is better than CNP because of being coated with polymer which is not thermally stable.

3.1.5. Magnetic properties

The magnetic properties of NP and CNP were investigated with a VSM at room temperature and the results are given in Fig. 5(a) and (b). In the magnetization curves, any hysteresis and symmetry about the origin were not observed. This meant that the samples have paramagnetic behavior. The saturation magnetization (m_s) values for NP and CNP were 29.5 and 18.25 emu/g at room temperature, respectively. The saturation magnetization of the particle can be affected by their structure, such as size and crystallinity. The saturation magnetization values of the samples decreased along with the formation of the polymeric coatings. However, the magnetism of the samples was still effective enough for them to be easily and quickly separated from the suspensions.

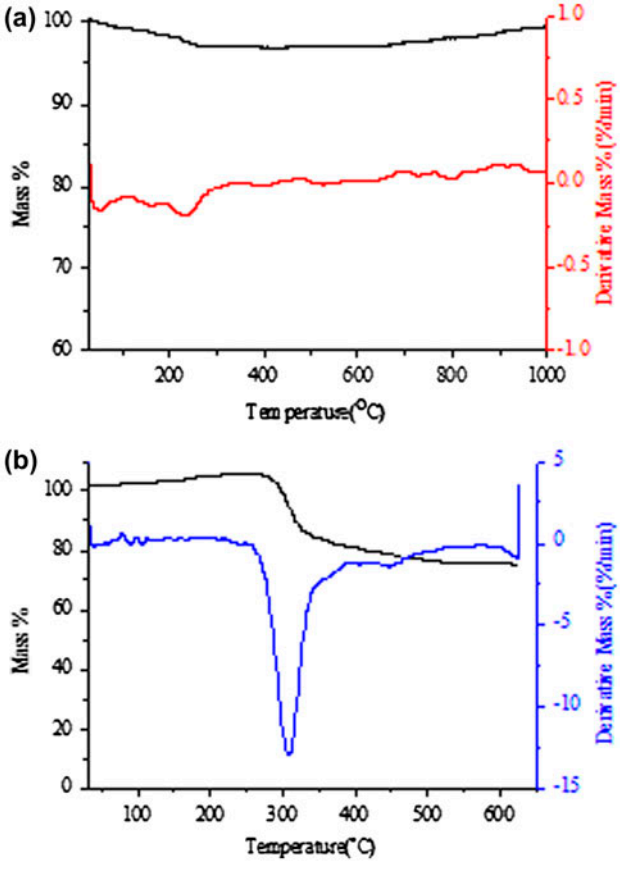

Fig. 4. TG curves of (a) NP and (b) CNP at nitrogen atmosphere.

3.2. Adsorption isotherms

The linear isotherm equations of Langmuir, Freundlich, Dubinin–Radushkevich (DR), and Brunauer–Emmett–Teller (BET) were used to evaluate the adsorption data. The results are given in Table 1. As depicted in Table 1 and Fig. 6, it was found that the adsorption of Cu(II) on the CNP was fitted with the Langmuir equation (R^2 = 0.9993) as compared to other isotherm equations. According to the R_L value, the sorption of the Cu(II) is favorable and also, the mono layer capacity was determined as 502.5 mg/g at which the result has been compatible with experimental data.

3.3. Kinetic studies

The adsorption capacity of CNP increased with the increase in contact time from 0 to 180 min. The

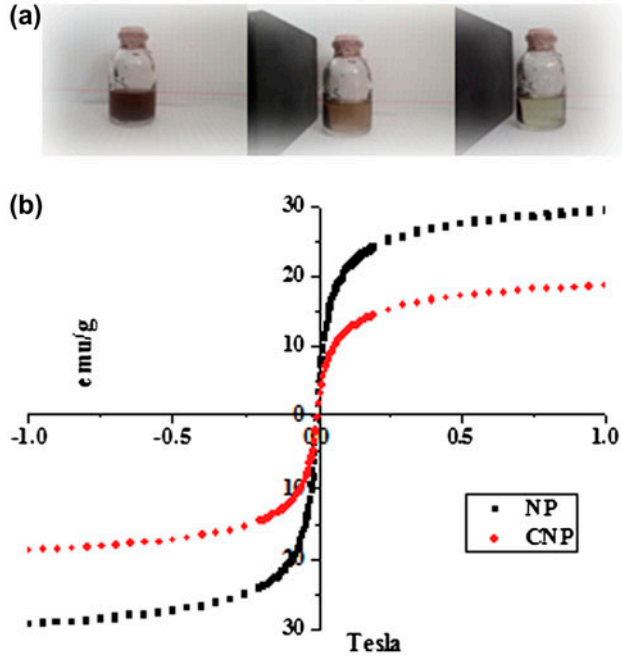

Fig. 5. The VSM curves of (a) NP and (b) CNP.

Table 1
Adsorption data

Langmuir $\frac{C_e}{q_e}=\frac{1}{q_m L}+\frac{C_e}{q_m}$	q_{exp} (mg/g)	q_{max} (mg/g)	R_L	R^2
	500	502.5	0.00047	0.9993
Freundlich $\ln q_e = \ln K_f + \frac{1}{n_f}\ln C_e$	q_{exp} (mg/g)	K_f (mg/g)	n_f	R^2
	500	239.4	200	0.8291
$\ln q_e = \ln X_m - \beta^2$Dubinin – Radushkevich (DR) $\ln q_e = \ln X_m - \beta\varepsilon^2$	q_{exp} (mg/g)	X_m (mg/g)	E (kJ/mg)	R^2
	500	458.2	1.581	0.9366
Brunauer–Emmett–Teller (BET) $\frac{C_e}{(C_i-C_e)q_e}=\frac{1}{Bq_{max}}+\frac{B-1}{Bq_{max}}\left(\frac{C_e}{C_i}\right)$	q_{exp} (mg/g)	q_{max} (mg/g)	B (J)	R^2
	500	526	1.00526	0.9986

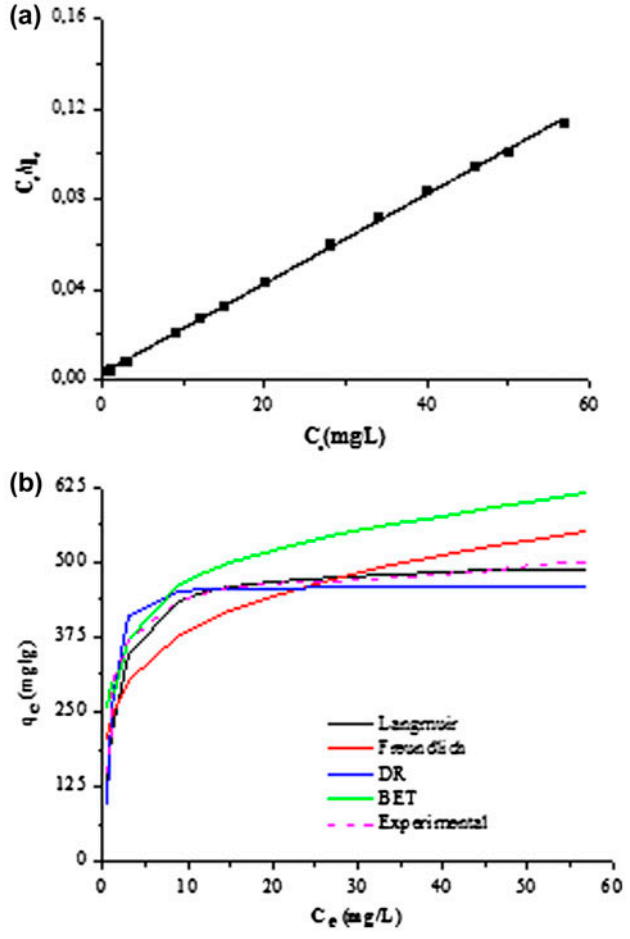

Fig. 6. (a) Linear curve of Langmuir isotherm and (b) the suitability equilibrium data in Freundlich, Langmuir, DR, and BET isotherms at 308 K.

equilibrium adsorption capacity for Cu(II) reached to 95% within 120 min. Then, the adsorption capacity becomes constant. In order to investigate the mechanism of sorption processes, several kinetic equations were used. Applied kinetic equations and results of the equations are given in Table 2. In accordance with the results, the pseudo-second-order kinetic model was found to be the best (Fig. 7). It may be said that the rate-limiting step may be chemical sorption or chemisorption involving valency forces through sharing or exchange of electrons between the sorbent and sorbate [31]. The experimental (q_{exp}) and calculated (q_e) adsorption capacities were determined as 499 and 555 mg/g, respectively.

3.4. Influence of pH value onto sorption

The adsorption capacity of an adsorbent is affected by the pH value of the solution. Therefore, adsorption of Cu(II) ions onto CNP was studied at pH 2–6 (Fig. 8). The adsorption studies at pH > 6 were not tested due to the precipitation of Cu(II) ions as $Cu(OH)_2$. It is clearly seen in Fig. 8 that the adsorption capacity of CNP increased with an increase in pH value. This increase could be explained that more protons will be available at low pH to interact with amine groups by forming $-NH_3^+$ and reducing the number of binding sites for the adsorption. On the other hand, adsorption of Cu(II) increases at higher pH. This is because of the decrease in the inhibitory effect of proton with the increase in pH [36].

The other reason for increase in the adsorption capacity at higher solution pH is the possible reaction between $-NH_2$ and $-OH^-$ might proceed as $-NH_2OH^-$. This electrostatic attraction reaction might raise the adsorption of Cu(II) as in the below equation:

$$-NH_2OH^- + Cu^{2+}(\text{or } CuOH^+) \rightarrow NH_2OH^-\ldots Cu^{2+}(\text{or } -NH_2OH^-\ldots CuOH^+)$$

Table 2
The results of kinetic studies

The pseudo-second-order $\frac{t}{q_t}=\frac{1}{k_2 q_e^2}+\frac{t}{q_e}$	q_{exp} (mg/g)	k (L/mg/min)	h (mg/g min)	q_e (mg/g)	R^2
	499	4.27×10^{-4}	13.19	555	0.9991
Lagergren-first-order $\ln(q_e - q_t) = \ln q_e - k_1 t$	q_{exp} (mg/g)	k (s^{-1})	q_e (mg/g)		R^2
	499	7.13×10^{-3}	471		0.9442
Elovich equation $q_t = \frac{1}{\beta}\ln\beta\alpha + \frac{1}{\beta}\ln t$	q_{exp} (mg/g)	α (mg/g min)	β (g/mg)		R^2
	499	32.41	8.73×10^{-3}		0.9909
Intra- particle diffusion $q_t = k_i t^{0.5} + C$	q_{exp} (mg/g)	k_i (mg/g $min^{0.5}$)	C (mg/g)		R^2
	499	34.624	24.784		0.9585

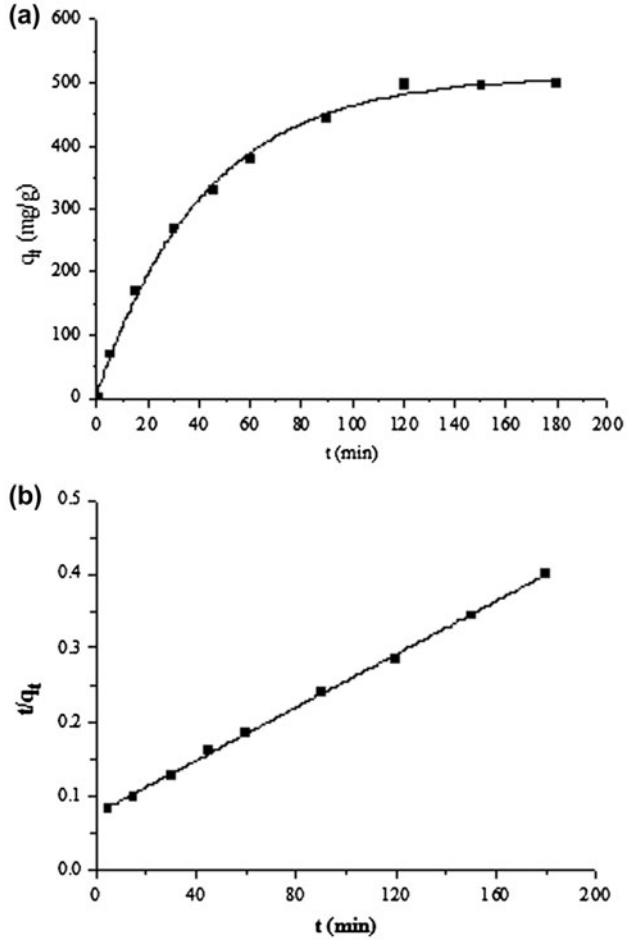

Fig. 7. (a) Contact time of adsorption study for CNP and (b) linear curve of the pseudo-second-order.

3.5. Thermodynamics of adsorption studies

Thermodynamic parameters ΔG°, ΔH°, and ΔS° and equilibrium constant K_d were determined using the following equations [50–54]:

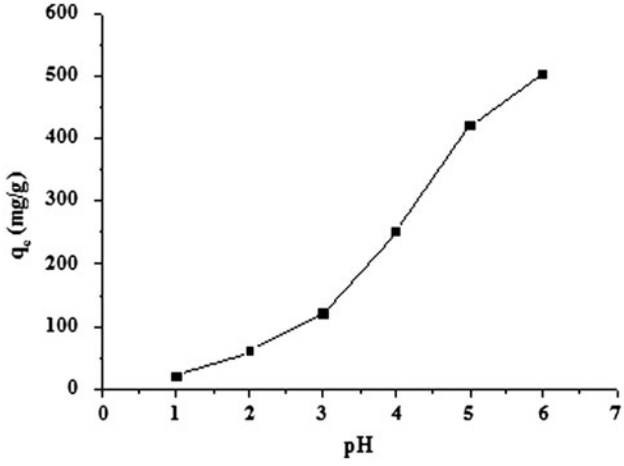

Fig. 8. Effect of pH on the adsorption.

$$\Delta G^\circ = -RT \ln K_d \quad (3)$$

$$K_d = q_e/C_e \quad (4)$$

$$\ln K_d = -\Delta H^\circ/RT + \Delta S^\circ/R \quad (5)$$

where R is 8.314 J/mol K, T is the temperature in K, q_e is the amount of Cu(II) (mg) adsorbed by one gram of CNP at equilibrium, and C_e is the equilibrium concentration (mg/L) of Cu(II) in solution.

$\ln K_d$ vs. $1/T$ plot is presented in Fig. 9. The slope and intercept of the line are equal to $\Delta S^\circ/R$ and $\Delta H^\circ/R$, respectively. The parameters are given in Table 3. A positive ΔH° value indicates the endothermic nature of the sorption. The value of ΔH° was obtained to be 127.4 kJ/mol and falls into the range of 80–200 kJ/mol which indicates the chemisorption [55].

Negative ΔG° values indicate that adsorption of Cu(II) ions onto CNP is favorable and spontaneous. ΔG° values decreased from −8.41 to −172.88 kJ/mol with increasing temperature. This means that

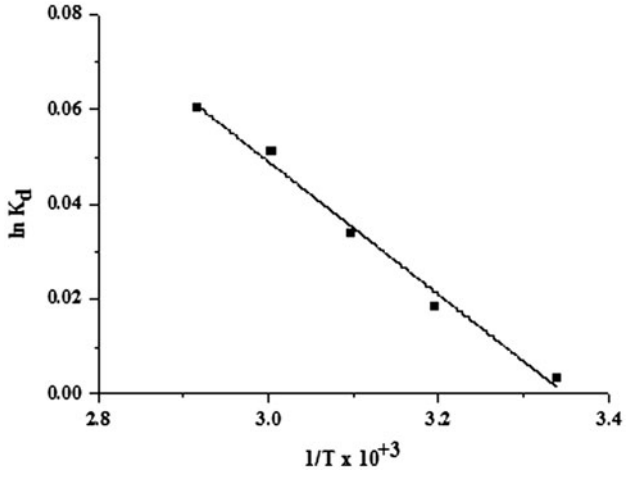

Fig. 9. ln K_d vs. $1/T$ Graph.

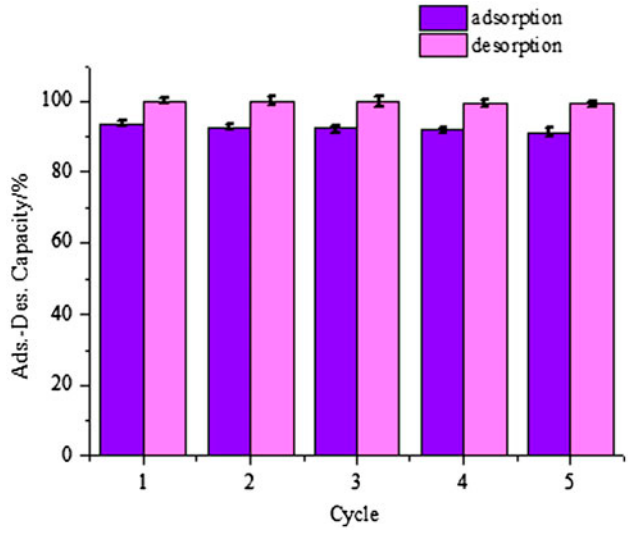

Fig. 10. Adsorption and desorption capacity of CNP in the reusability experiments (initial concentration of Cu(II) ions was 500 mg/L at pH 6.0).

Table 3
Thermodynamic parameters for adsorption of Cu^{2+} on CNP

T (K)	ΔG (J/mol)	ΔH (kJ/mol)	ΔS (J/mol)
303	−8.41	127.37	4.23
313	−48.49		
323	−91.04		
333	−142.01		
343	−172.88		

adsorption was more spontaneous at higher temperatures [56].

It is clear that ΔG° value, up to −20 kJ/mol, indicates physisorption, while −40 kJ/mol indicates chemisorption. ΔG° value between −20 and −40 kJ/mol indicates that both physisorption and chemisorption were responsible for adsorption. Positive ΔS° values point out the randomness at the solid/solution interface during the adsorption of Cu (II) on CNP. The adsorbed water molecules, which are displaced by the adsorbate species, gain more translational entropy than is lost by the adsorbate molecules, thus allowing the prevalence of randomness in the system [57].

3.6. Reusability studies of the adsorbent

The recycling of adsorbed material and reusability of the adsorbents are very important in the points of views of adsorption, desorption and recovery of the metal ions.

It has been clearly seen in the pH study that the adsorption of Cu(II) onto CNP at pH 1 was insignificant. Therefore, desorption of Cu(II) from CNP was reasonable in this pH. HNO_3 solution was used as desorption agent due to its act as a cation exchanger agent. The reusability was checked by following the adsorption–desorption processes for five cycles. The adsorption efficiency in each cycle was analyzed. The adsorption study was followed by 0.01 g of CNP with 15 mL of 400 mg/L copper ion solution at pH 6 for 120 min at 200 rpm at 30°C. The desorption study was conducted in the HNO_3 solution at pH 1.0 as mentioned

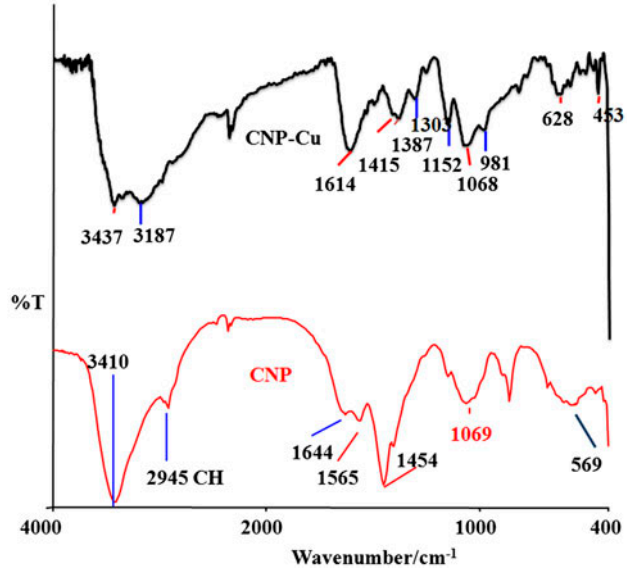

Fig. 11. FTIR spectrum of CNP after Cu(II) ion adsorption.

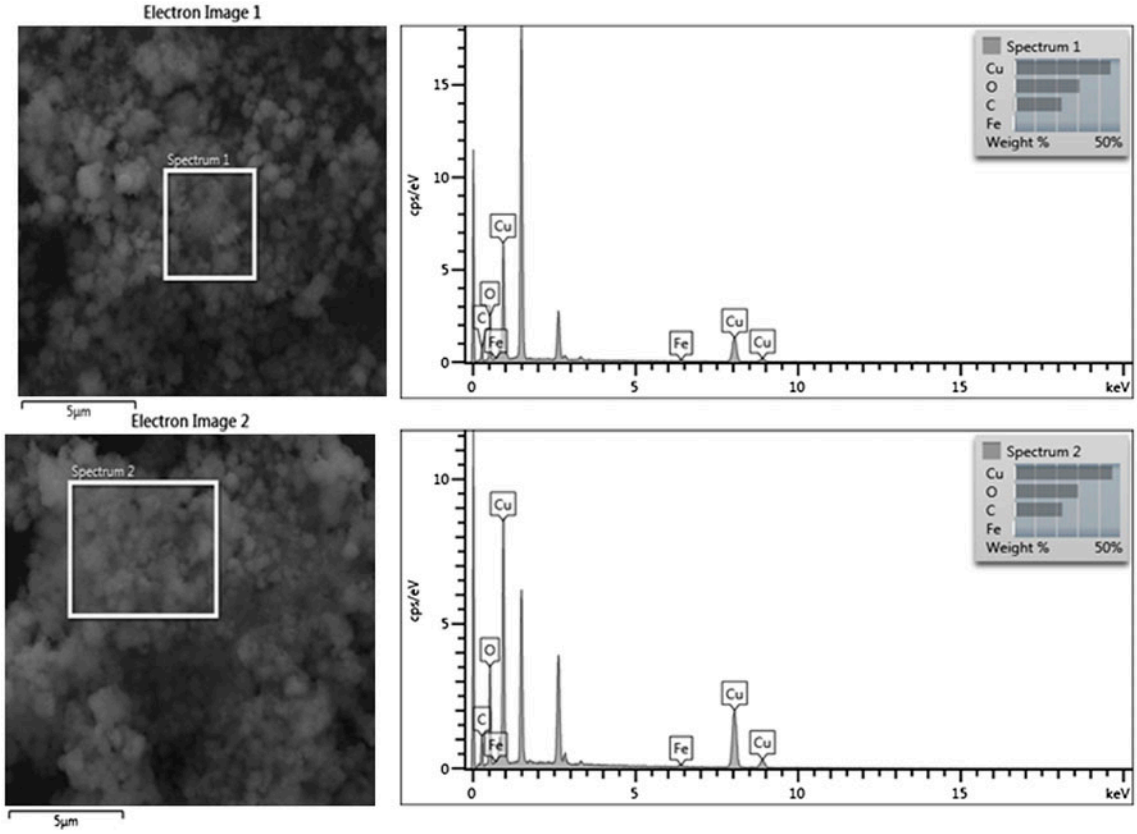

Fig. 12. SEM images of CNP after Cu(II) ion adsorption and EDX analysis.

above. As shown in Fig. 10, the adsorption percentages were 93.6, 92.8, 92.25, 91.84, and 91.12% in the adsorption–desorption cycles, respectively. Thus, the CNP adsorbent can be reused successfully five times after regeneration for Cu(II) ion adsorption from aqueous solution, almost without any significant loss in the adsorption capacity.

3.7. Characterization of CNP After Cu(II) adsorption

In Fig. 11, the spectrum of CNP displays a broad band at 3,410 cm^{-1}, which corresponds to the stretching vibration of O–H and extension vibration of N–H. The band shifted to 3,437 and 3,187 cm^{-1} after adsorption of Cu(II), which implies that O and N atoms played a role in the uptake of metal ions. On the other hand, from the spectrum of CNP after adsorption, a new adsorption band appeared at 1,387 cm^{-1}, which was caused by the bond flexion of C–O–H where the oxygen atom (in O–H) forms a coordination bond with Cu(II). Furthermore, the band of Fe–O (569 cm^{-1}) shifted to 628 cm^{-1} after adsorption of Cu(II), which implied that Fe–O and Cu–O groups played a role in the uptake of metal ions.

Table 4
SEM–EDX results of CNP after Cu(II) adsorption

	1st Spectrum		2nd Spectrum	
Element	Wt.%	Atomic %	Wt.%	Atomic %
C	22.59	41.34	22.87	41.96
O	30.96	42.54	30.34	41.79
Fe	0.95	0.37	0.44	0.17
Cu	45.50	15.74	46.34	16.07
Total	100.00	100.00	100.00	100.00

The other characterization of CNP after Cu(II) adsorption is EDX analysis for determination of CNP per gram amount of adsorbed Cu(II) (mg). As the result of EDX analysis (Fig. 12 and Table 4) for two different parts of the CNP after adsorption, the amount of adsorbed Cu(II) was determined as 45.50 and 46.34%. Furthermore, the particle size of the CNP after adsorption has increased from 26 to 443 nm. Additionally, when EDX results (average 459.2 mg/g) compared with experimental results (average 495 mg/g), the approximate values were calculated.

Table 5
Comparison of adsorbent capacities for Cu(II) ion adsorption

Adsorbent	Adsorption capacity (mg/g)	Refs.
Chitosan-/PVA-coated magnetic nanoadsorbent	502.5	In this study
Gum arabic-modified magnetic nanoadsorbent	38.5	[30]
Chitosan-coated magnetic nanoparticles	44.9	[58]
Chitosan-coated magnetic nanoparticles	35.5	[59]
Chitosan-bound Fe_3O_4	21.50	[60]
Carboxymethyl–cyclodextrin conjugated magnetic nanoparticles	47.2	[61]
Magnetic nanoadsorbent (MNP-NH_2)	25.77	[62]
Magnetite nanoparticles	35.46	[63]
Chitosan-coated magnetic nanoparticles	144.9	[58]
(Mnp-NH_2)	25.77	[62]
Magnetic ion-imprinted composite adsorbent	46.25	[64]
Lentil (LS), wheat (WS), and rice (RS)	8.977, 9.510, and 9.588	[65]
Tamarindus indica seed powder	133.24	[66]
Tamarindus indica fruit shell	80.01	[67]

4. Conclusions

The characterization of CNP indicated that Fe_3O_4-NP have been introduced successfully in CNP without destroying the general crystal structure of NP. In the comparison of the isotherm equations applied to the experimental data, Langmuir isotherm is the best fitted isotherm among the other isotherm models. As far as the adsorption kinetics is concerned, the pseudo-second-order kinetic model fitted the data well. On the other hand, thermodynamics of the adsorption resulted to be spontaneous and endothermic in nature. The adsorption capacity of Cu(II) sorption onto CNP was found to be 500 mg/g. The Cu(II) ions can be easily desorbed from CNP by treatment with HNO_3 solution. The saturation magnetization values of CNP decreased due to the formation of the polymeric coatings. However, the magnetism was still effective enough for easy and quick separation. The compared adsorption capacity of CNP with the other adsorbents is shown in Table 5. It can be clearly seen that the capacity of CNP is the highest rather than the others. The adsorption–desorption cycles were also sufficient for the usage of these adsorbents. It can be concluded that CNP can be used as an adsorbent in the wastewater treatment with an easy magnetic separation and convenient recovery.

Acknowledgment

This work was supported by the Dokuz Eylül University Research Foundation (grant number 2014.KB.FEN.009).

References

[1] P. Pal, F. Banat, Comparison of heavy metal ions removal from industrial lean amine solvent using ion exchange resins and sand coated with chitosan, J. Nat. Gas Sci. Eng. 18 (2014) 227–236.
[2] T. Benvenuti, M.A.S. Rodrigues, A.M. Bernardes, J.Z. Ferreira, Electrodialysis treatment of nickel wastewater, in: Electrodialysis and Water Reuse, Springer, Berlin, Heidelberg, 2014, pp. 133–144.
[3] Y. Ge, Z. Li, Y. Kong, Q. Song, K. Wang, Heavy metal ions retention by bi-functionalized lignin: Synthesis, applications, and adsorption mechanisms, J. Ind. Eng. Chem. 20(6) (2014) 4429–4436.
[4] M. Kumar, B.P. Tripathi, V.K. Shahi, Crosslinked chitosan/polyvinyl alcohol blend beads for removal and recovery of Cd(II) from wastewater, J. Hazard. Mater. 172(2–3) (2009) 1041–1048.
[5] S. Zhang, Y. Zhou, W. Nie, L. Song, Preparation of Fe_3O_4/chitosan/poly (acrylic acid) composite particles and its application in adsorbing copper ion (II), Cellulose 19(6) (2012) 2081–2091.
[6] W. Jiang, W. Wang, B. Pan, Q. Zhang, W. Zhang, L. Lv, Facile fabrication of magnetic chitosan beads of fast kinetics and high capacity for copper removal, ACS Appl. Mater. Interfaces 6(5) (2014) 3421–3426.
[7] H. Yan, L. Yang, Z. Yang, H. Yang, A. Li, R. Cheng, Preparation of chitosan/poly(acrylic acid) magnetic composite microspheres and applications in the removal of copper(II) ions from aqueous solutions, J. Hazard. Mater. 229 (2012) 371–380.
[8] W. Wan Ngah, L.C. Teong, M. Hanafiah, Adsorption of dyes and heavy metal ions by chitosan composites: A review: Carbohydr. Polym., 83(4) (2011) 1446–1456.
[9] H. Liu, F. Yang, Y. Zheng, J. Kang, J. Qu, J.P. Chen, Improvement of metal adsorption onto chitosan/*Sargassum* sp. composite sorbent by an innovative ion-imprint technology, Water Res. 45(1) (2011) 145–154.
[10] H.V. Tran, L.D. Tran, T.N. Nguyen, Preparation of chitosan/magnetite composite beads and their

application for removal of Pb(II) and Ni(II) from aqueous solution, Mater. Sci. Eng. C 30(2) (2010) 304–310.
[11] D. Reddy, S.M. Lee, Application of magnetic chitosan composites for the removal of toxic metal and dyes from aqueous solutions, Adv. in Colloid Interface Sci. 201 (2013) 68–93.
[12] A.H. Latham, M.E. Williams, Controlling transport and chemical functionality of magnetic nanoparticles, Acc. Chem. Res. 41 (2008) 411–420.
[13] M.S. Toprak, B.J. McKenna, M. Mikhaylova, J.H. Waite, G.D. Stucky, Spontaneous assembly of magnetic microspheres, Adv. Mater. 19 (2007) 1362–1368.
[14] R.D. Ambashta, M. Sillanpää, Water purification using magnetic assistance: A review, J. Hazard. Mater. 180 (1) (2010) 38–49.
[15] C.T. Yavuz, J.T. Mayo, W.W. Yu, A. Prakash, J.C. Falkner, S. Yean, L.L. Cong, H.J. Shipley, A. Kan, M. Tomson, D. Natelson, V.L. Colvin, Low-field magnetic separation of monodisperse Fe_3O_4 nanocrystals, Science 314 (2006) 964–967.
[16] M.A. Shannon, P.W. Bohn, M. Elimelech, J.G. Georgiadis, B.J. Mariñas, A.M. Mayes, Science and technology for water purification in the coming decades, Nature 452 (2008) 301–310.
[17] Z.H. Ai, Y. Cheng, L.Z. Zhang, J.R. Qiu, Efficient removal of Cr(VI) from aqueous solution with $Fe@Fe_2O_3$ core-shell nanowires, Environ. Sci. Technol. 42 (2008) 6955–6960.
[18] T. Tuutijärvi, J. Lu, M. Sillanpää, G. Chen, As(V) adsorption on maghemite nanoparticles, J. Hazard. Mater. 166 (2009) 1415–1420.
[19] W. Yantasee, C.L. Warner, T. Sangvanich, R.S. Addleman, T.G. Carter, R.J. Wiacek, G.E. Fryxell, C. Timchalk, M.G. Warner, Removal of heavy metals from aqueous systems with thiol functionalized superparamagnetic nanoparticles, Environ. Sci. Technol. 41 (2007) 5114–5119.
[20] A.M. Donia, A.A. Atia, K.Z. Elwakeel, Selective separation of mercury(II) using magnetic chitosan resin modified with Schiff's base derived from thiourea and glutaraldehyde, J. Hazard. Mater. 151 (2008) 372–379.
[21] D. Hritcu, D. Humelnicu, G. Dodi, M.I. Popa, Magnetic chitosan composite particles: Evaluation of thorium and uranyl ion adsorption from aqueous solutions, Carbohydr. Polym. 87(2) (2012) 1185–1191.
[22] Z. Zhou, S. Lin, T. Yue, T.C. Lee, Adsorption of food dyes from aqueous solution by glutaraldehyde crosslinked magnetic chitosan nanoparticles, J. Food Eng. 126 (2014) 133–141.
[23] A.K. Gupta, M. Gupta, Synthesis and surface engineering of iron oxide nanoparticles for biomedical applications, Biomaterials 26(18) (2005) 3995–4021.
[24] T.R. Pisanic, J.D. Blackwell, V.I. Shubayev, R.R. Fiñones, S. Jin, Nanotoxicity of iron oxide nanoparticle internalization in growing neurons, Biomaterials 28(16) (2007) 2572–2581.
[25] E.A. Deliyanni, D.N. Bakoyannakis, A.I. Zouboulis, K.A. Matis, Sorption of As(V) ions by akaganéite-type nanocrystals, Chemosphere 50 (2003) 155–163.
[26] M. Ajmal, A.H. Khan, S. Ahmad, A. Ahmad, Role of sawdust in the removal of copper(II) from industrial wastes, Water Res. 32 (1998) 3085–3091.
[27] S. Deng, R. Bai, J.P. Chen, Aminated polyacrylonitrile fibers for lead and copper removal, Langmuir 19 (2003) 5058–5064.
[28] C. Sun, R. Qu, C. Ji, C. Wang, Y. Sun, Z. Yue, G. Cheng, Preparation and adsorption properties of crosslinked polystyrene-supported low-generation diethanolamine-typed dendrimer for metal ions, Talanta 70 (2006) 14–19.
[29] Y.C. Chang, D.H. Chen, Preparation and adsorption properties of monodisperse chitosan-bound Fe_3O_4 magnetic nanoparticles for removal of Cu(II) ions, J. Colloid Interface Sci. 283 (2005) 446–451.
[30] S.S. Banerjee, D.H. Chen, Fast removal of copper ions by gum arabic modified magnetic nano-adsorbent, J. Hazard. Mater. 147(3) (2007) 792–799.
[31] Y.M. Hao, C. Man, Z.B. Hu, Effective removal of Cu(II) ions from aqueous solution by amino-functionalized magnetic nanoparticles, J. Hazard. Mater. 184 (2010) 392–399.
[32] Y.H. Chen, F.A. Li, Kinetic study on removal of copper(II) using goethite and hematite nano-photocatalysts, J. Colloid Interface Sci. 347(2) (2010) 277–281.
[33] A. Findon, G. McKay, H.S. Blair, Transport studies for the sorption of copper ions by chitosan, J. Environ. Sci. Health A 28 (1993) 173–185.
[34] W.H. Cheung, J.C.Y. Ng, G. Mckay, Kinetic analysis of the sorption of copper(II) ions on chitosan, J. Chem. Technol. Biotechnol. 78 (2003) 562–571.
[35] C. Huang, Y.C. Chung, M.-R. Liou, Adsorption of Cu(II) and Ni(II) by pelletized biopolymer, J. Hazard. Mater. 45 (1996) 265–277.
[36] W.S.W. Ngah, C.S. Endud, R. Mayanar, Removal of copper(II) ions from aqueous solution onto chitosan and cross-linked chitosan beads, React. Funct. Polym. 50 (2002) 181–190.
[37] S.R. Popuri, Y. Vijaya, V.M. Boddu, K. Abburi, Adsorptive removal of copper and nickel ions from water using chitosan coated PVC beads, Bioresour. Technol. 100 (2009) 194–199.
[38] S. Tan, Y. Wang, C. Peng, Y. Tang, Synthesis and adsorption properties for metal ions of crosslinked chitosan acetate crown ethers, J. Appl. Polym. Sci. 71 (1999) 2069–2074.
[39] B. Kannamba, K.L. Reddy, B.V. Appa Rao, Removal of Cu(II) from aqueous solutions using chemically modified chitosan, J. Hazard. Mater. 175 (2010) 939–948.
[40] S.M. Zhu, N. Yang, D. Zhang, Poly(N,N-dimethylaminoethyl methacrylate) modification of activated carbon for copper ions removal, Mater. Chem. Phys. 113 (2009) 784–789.
[41] G.P. Rao, C. Lu, F. Su, Sorption of divalent metal ions from aqueous solution by carbon nanotubes: A review, Sep. Purif. Technol. 58 (2007) 224–231.
[42] P. Yin, Q. Xu, R.J. Qu, G.F. Zhao, Removal of transition metal ions from aqueous solutions by adsorption onto a novel silica gel matrix composite adsorbent, J. Hazard. Mater. 169 (2009) 228–232.
[43] Y. Chen, J. Hu, J. Wang, Kinetics and thermodynamics of Cu(II) biosorption on to a novel magnetic chitosan composite bead, Environ. Technol. 33 (2012) 2345–2351.
[44] J. Brugnerotto, J. Lizardi, F.M. Goycoolea, W. Argüelles-Monal, J. Desbrières, M. Rinaudo, An

infrared investigation in relation with chitin and chitosan characterization, Polymer 42 (2001) 3569–3580.
[45] P.C. Srinivasa, M.N. Ramesh, K.R. Kumar, R.N. Tharanathan, Properties and sorption studies of chitosan-polyvinyl alcohol blend films, Carbohydr. Polym. 53(4) (2003) 431–438.
[46] Y.C. Chang, D.H. Chen, Preparation and adsorption properties of monodisperse chitosan-bound Fe_3O_4 magnetic nanoparticles for removal of Cu(II) ions, J. Colloid Interface Sci. 283 (2005) 446–451.
[47] G.Y. Li, Y.R. Jiang, K.L. Huang, P. Ding, J. Chen, Preparation and properties of magnetic Fe_3O_4–chitosan nanoparticles, J. Alloys Compd. 466 (2008) 451–456.
[48] J. Zhi, Y. Wang, Y. Lu, J. Ma, G. Luo, In situ preparation of magnetic chitosan/Fe_3O_4 composite nanoparticles in tiny pools of water-in-oil microemulsion, React. Funct. Polym. 66 (2006) 1552–1558.
[49] W.S.W. Ngah, A. Kamari, Y.J. Koay, Equilibrium and kinetics studies of adsorption of copper(II) on chitosan and chitosan/PVA beads, Int. J. Biol. Macromol. 34(3) (2004) 155–161.
[50] S.K. Milonjic, A consideration of the correct calculation of thermodynamic parameters of adsorption, J. Serb. Chem. Soc. 72(12) (2007) 1363–1367.
[51] A. Altinisik, K. Yurdakoc, Chitosan/poly(vinyl alcohol) hydrogels for amoxicillin release, Polym. Bull. 71 (3) (2014) 759–774.
[52] E. Akar, A. Altinişik, Y. Seki, Using of activated carbon produced from spent tea leaves for the removal of malachite green from aqueous solution, Ecol. Eng. 52 (2013) 19–27.
[53] D.G. Krishna, G. Bhattacheryya, Adsorption of methylene blue on kaolinite, Appl. Clay Sci. 20 (2002) 295–303.
[54] A. Khenifi, Z. Bouberka, F. Sekrane, M. Kameche, Z. Derriche, Adsorption study of an industrial dye by an organic clay, Adsorption 13 (2007) 149–158.
[55] Y. Liu, Y.J. Liu, Biosorption isotherms, kinetics and thermodynamics, Sep. Purif. Technol. 61 (2008) 229–242.
[56] B.S. Chu, B.S. Baharin, Y.B. Che Man, S.Y. Quek, Separation of vitamin E from palm fatty acid distillate using silica. I. Equilibrium of batch adsorption, J. Food Eng. 62 (2004) 97–103.
[57] C. Namasivayam, D. Kavitha, Removal of Congo Red from water by adsorption onto activated carbon prepared from coir pith, an agricultural solid waste, Dyes Pigm. 54 (2002) 47–58.
[58] Q. Peng, Y. Liu, G. Zeng, W. Xu, C. Yang, J. Zhang, Biosorption of copper(II) by immobilizing *Saccharomyces cerevisiae* on the surface of chitosan-coated magnetic nanoparticles from aqueous solution, J. Hazard. Mater. 177(1–3) (2010) 676–682.
[59] C. Yuwei, W. Jianlong, Preparation and characterization of magnetic chitosan nanoparticles and its application for Cu(II) removal, Chem. Eng. J. 168(1) (2011) 286–292.
[60] Y.C. Chang, D.H. Chen, Preparation and adsorption properties of monodisperse chitosan-bound Fe_3O_4 magnetic nanoparticles for removal of Cu(II) ions, J. Colloid Interface Sci. 283(2) (2005) 446–451.
[61] A.Z.M. Badruddoza, A.S.H. Tay, P.Y. Tan, K. Hidajat, M.S. Uddin, Carboxymethyl-β-cyclodextrin conjugated magnetic nanoparticles as nano-adsorbents for removal of copper ions: Synthesis and adsorption studies, J. Hazard. Mater. 185(2–3) (2011) 1177–1186.
[62] Y.M. Hao, C. Man, Z.B. Hu, Effective removal of Cu (II) ions from aqueous solution by amino-functionalized magnetic nanoparticles, J. Hazard. Mater. 184(1–3) (2010) 392–399.
[63] Y.F. Shen, J. Tang, Z.H. Nie, Y.D. Wang, Y. Ren, L. Zuo, Preparation and application of magnetic Fe_3O_4 nanoparticles for wastewater purification, Sep. Purif. Technol. 68(3) (2009) 312–319.
[64] Y. Ren, X. Wei, M. Zhang, Adsorption character for removal Cu(II) by magnetic Cu(II) ion imprinted composite adsorbent, J. Hazard. Mater. 158(1) (2008) 14–22.
[65] H. Aydın, Y. Bulut, Ç. Yerlikaya, Removal of copper(II) from aqueous solution by adsorption onto low-cost adsorbents, J. Environ. Manage. 87(1) (2008) 37–45.
[66] S. Chowdhury, P.D. Saha, Biosorption kinetics, thermodynamics and isosteric heat of sorption of Cu(II) onto *Tamarindus indica* seed powder, Colloids Surf., B: Biointerfaces 88(2) (2011) 697–705.
[67] S. Chowdhury, P.D. Saha, Batch and continuous (fixed-bed column) biosorption of Cu(II) by *Tamarindus indica* fruit shell, Korean J. Chem. Eng. 30 (2) (2013) 369–378.